

# Modeling dynamics of AIR-1, ECT-2, and myosin in polarity establishment and cytokinesis

Ondrej Maxian

March 18, 2024

## 1 The centrosome cue

The contractility circuit is forced by a cue from the centrosomes which contain Aurora A (AIR-1), an inhibitor of ECT-2. We assume that the AIR-1 signal gets to the membrane by diffusion. Letting  $a(\mathbf{x})$  be the concentration of AIR-1 in the embryo, we have the equation

$$\Delta a = -f \quad \mathbf{x} \in \Omega \quad (1a)$$

$$\nabla a \cdot \mathbf{n} = 0 \quad \mathbf{x} \in \partial\Omega, \quad (1b)$$

where (1a) is the diffusion equation for the concentration and (1b) is a no-flux boundary condition through the boundary (here  $\Omega$  represents the embryo area and  $\partial\Omega$  represents the boundary). The signal  $f(\mathbf{x})$  comes from the two centrosomes, which we model by Gaussian densities

$$f(\mathbf{x}) = \frac{C_0/D}{2\pi\sigma_c^2} \sum_{i=1}^2 \exp\left(\frac{-\|\mathbf{x} - \mathbf{x}_i\|^2}{2\sigma_c^2}\right). \quad (1c)$$

Here  $\mathbf{x}_i$  is the location of the  $i$ th centrosome (typically at some location  $(x_i, 0)$ ), which changes depending on the embryo conditions. In addition to the centrosome location, the signal has two other parameters:  $C_0/D$  is the strength of the cue (the integral of  $f(\mathbf{x})$  over the entire embryo cross-section, normalized by the cytoplasmic diffusion coefficient  $D$ ), and  $\sigma_c$  is the centrosome “size” (the standard deviation of the Gaussian, which is roughly half the size of the centrosome). For cytokinesis, the centrosomes have size about  $2 \mu\text{m}$ , so we set  $\sigma_c = 1 \mu\text{m}$ . The solution of (1a) is unique up to a constant; thus, when we compare profiles to each other we can only speak of concentration *differences* rather than absolute concentration.

We use a standard first-order finite element method to solve (1a). In brief, the elliptical domain of the embryo is meshed into nodes and triangles, which define a set of linear Lagrangian basis

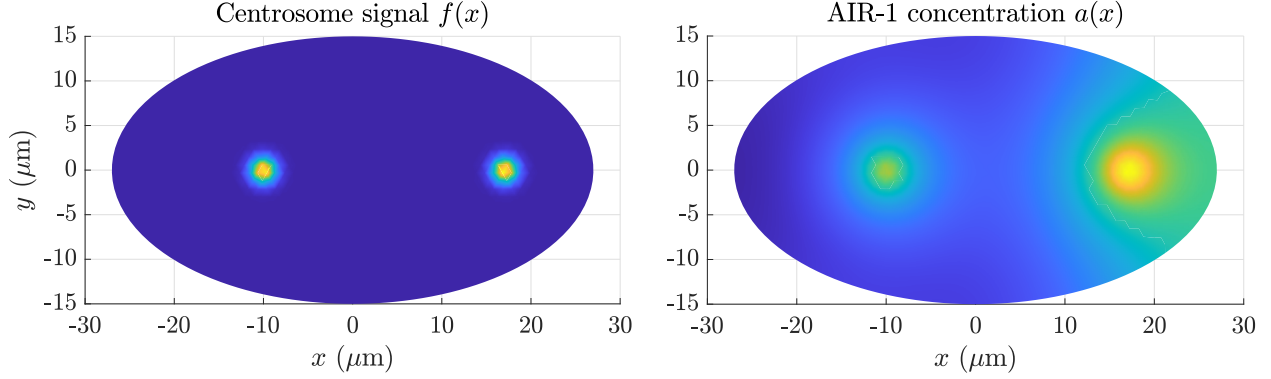


**Figure 1:** Solution for the diffusion equation (1) for wild-type embryos. The left panel shows the centrosome signal  $f(\mathbf{x})$ , with the anterior centrosome  $17 \mu\text{m}$  away from the anterior cortex and the posterior centrosome  $10 \mu\text{m}$  away from the posterior cortex. The Gaussian width  $\sigma_c = 1$  (so that the centrosome diameter is roughly  $2 \mu\text{m}$ ). The right panel shows the solution for the concentration profile  $a(\mathbf{x})$ .

functions  $\psi_k$  that are 1 at node  $\mathbf{x}_k$  and 0 everywhere else. Multiplying (1a) by a basis function  $\psi_k$ , then integrating by parts using the boundary condition (1b) gives

$$\sum_j \int_{\Omega} (\nabla \psi_k \cdot \nabla \psi_j) a_j d\mathbf{x} = \sum_j \int_{\Omega} \psi_k \psi_j f_j d\mathbf{x}, \quad (2)$$

which can be written as the matrix equation  $\mathbf{K}\mathbf{a} = \mathbf{M}\mathbf{f}$ , where  $\mathbf{M}$  is the so-called mass matrix and  $\mathbf{K}$  the stiffness matrix for finite elements. Solving  $\mathbf{a} = \mathbf{K}^\dagger \mathbf{M}\mathbf{f}$  gives the solution for the concentration.

Figure 1 shows the solution of the diffusion equation over the embryo cross-section in wild-type embryos. In this case, the anterior centrosome sits  $17 \mu\text{m}$  from the anterior pole, while the posterior centrosome sits  $10 \mu\text{m}$  from the posterior pole. The left panel shows the AIR-1 signal, which essentially shows the location of the two centrosomes. The right panel then shows the solution to the diffusion equation (1) in this case. As might be expected, there is substantially more AIR-1 on the anterior cortex, since the centrosome sits closer to the boundary there.

We now consider how moving the centrosomes changes the profile of AIR-1 on the boundary. We use six representative treatments from [7], which modify the positions of the centrosomes, and plot the results in Fig. 2. As an example, in *dhc-1* (RNAi) embryos, the posterior centrosome sits  $3 \mu\text{m}$  from the posterior pole, while the anterior centrosome sits  $45 \mu\text{m}$  from the anterior pole ( $9 \mu\text{m}$  from the posterior pole). As a result, the AIR-1 profile is strongly peaked at the posterior, with an AIR-1 gradient about 6 times larger than the wild-type. The treatments we consider

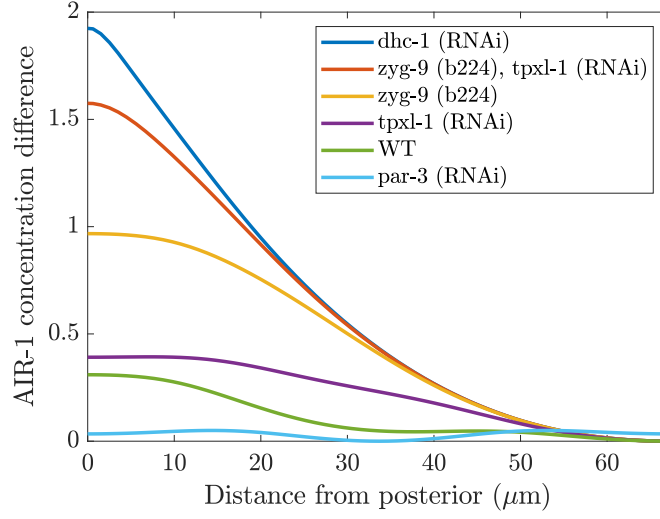


**Figure 2:** AIR-1 accumulation on the embryo perimeter (cortex) as predicted by the diffusion model (1). We show the AIR-1 profile as a function of distance from the posterior pole (0 is the posterior pole, 67 is the anterior pole), for embryos with six different treatments. The treatment sets the location of the centrosomes (see Fig. 5).

can also flatten the AIR-1 profile relative to wild-type, as in PAR-3 (RNAi) embryos, which have centrosomes sitting roughly at  $15 \mu\text{m}$  from each pole. The profile of AIR-1 there is consequently roughly constant.

### 1.1 Adding AIR-1 inactivation

We also consider the case when there is a basal level of inactivation of AIR-1 (phosphatase activity) in the cytoplasm. To model this, we modify (1a) to add an additional inactivation term

$$\Delta a - \bar{k}^{\text{off}} a = -f \quad \mathbf{x} \in \Omega. \quad (3)$$

This introduces another parameter which is the inactivation rate relative to the diffusion coefficient in the cytoplasm (units  $\mu\text{m}^{-2}$ ). Solving (3) with the finite element is very simple: the matrix equation becomes  $(\mathbf{K} + \bar{k}^{\text{off}} \mathbf{M}) \mathbf{a} = \mathbf{M} \mathbf{f}$ . An advantage of this approach is that the solution for concentration is unique (no longer an unknown constant).

Figure 3 shows the effect of the new inactivation term in the model, both in the cross-sectional profile of AIR-1, and also along the embryo perimeter from posterior to anterior. We find that  $\bar{k}^{\text{off}} \leq 10^{-3} \mu\text{m}^{-2}$  preserves the general trend we observed previously in wild-type embryos, where the concentration is about 0.3 units higher at the posterior than the anterior. Increasing the

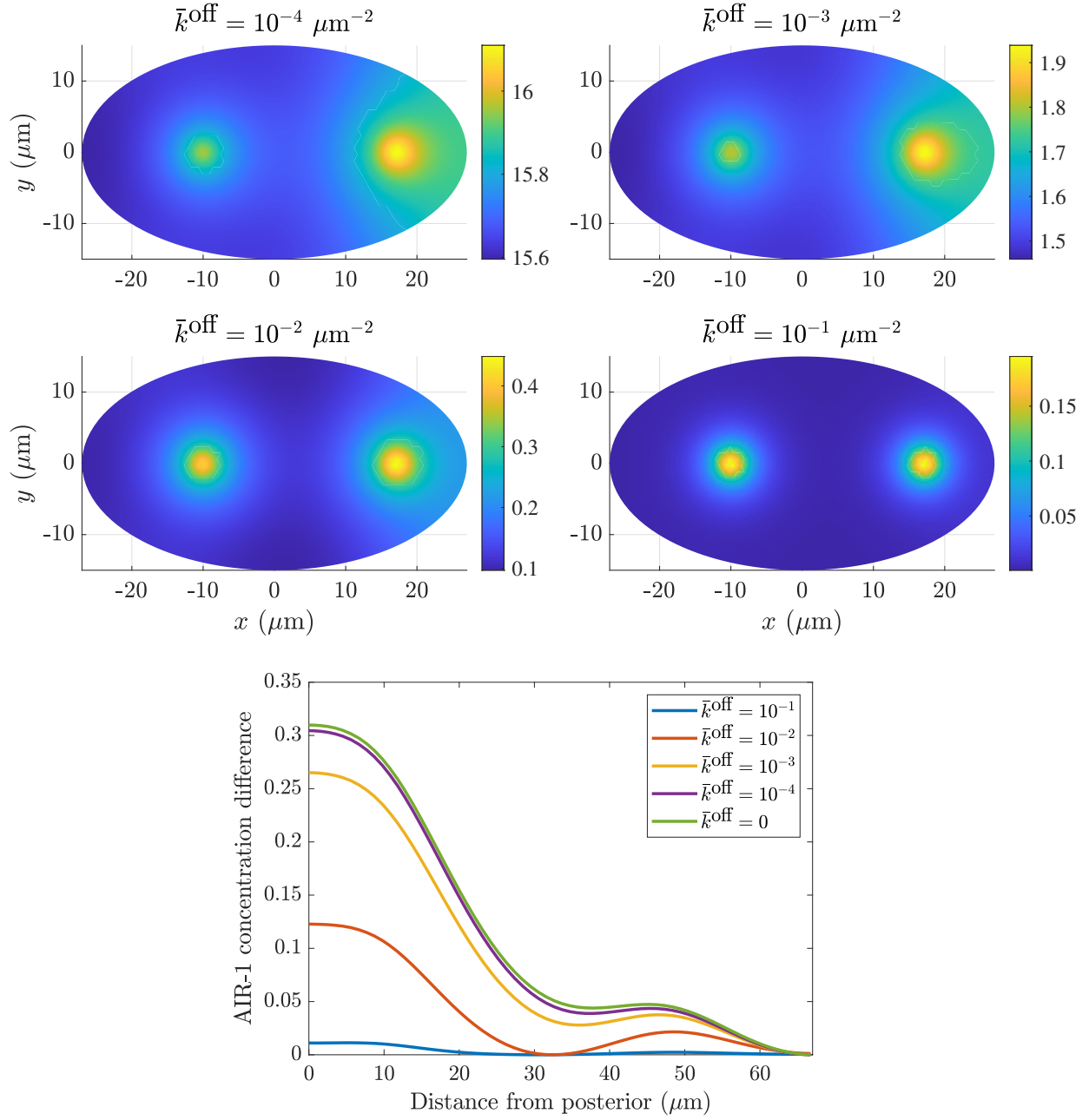


**Figure 3:** Profile of AIR-1 in wild-type embryo, obtained by solving (3) with different values of  $\bar{k}^{\text{off}} = k^{\text{off}}/D$ . The top plots show the profile along the whole embryo when changing  $\bar{k}^{\text{off}}$ ; the bottom (summary) plot shows the change in the AIR-1 concentration (relative to the anterior pole) along the embryo perimeter.

inactivation rate leads to more of the AIR-1 being inactivated prior to reaching the posterior pole, which causes the gradient to drop (for  $\bar{k}^{\text{off}} = 10^{-2} \mu\text{m}^{-2}$ ), and then vanish (for  $\bar{k}^{\text{off}} = 10^{-1} \mu\text{m}^{-2}$ ). In the cross-sectional views in Fig. 3, the colorbars show that the basal level of AIR-1 activity is roughly inversely proportional to  $\bar{k}^{\text{off}}$ ; increasing  $\bar{k}^{\text{off}}$  by a factor of 10 decreases the minimum AIR-1 concentration by a factor of 10. The high AIR-1 concentration for low  $\bar{k}^{\text{off}}$  models low phosphatase activity, in which case it was shown (after removing the centralspindlin-dependent pathway) that cells cannot form pseudocleavage due to low contractility [1, 6].

## 2 The ECT-2 response

Let us now examine how the strength of the AIR-1 signal affects the strength of the ECT-2 concentration on the proximal cortex. To do so, let us suppose that ECT-2 locally binds and unbinds from the cortex, with AIR-1 increasing the unbinding rate. At steady state, this gives the equation

$$k_E^{\text{on}} = k_E^{\text{off}} (1 + K_{\text{AE}} (A - A_{\text{min}})) E \rightarrow E = \frac{k_E^{\text{on}}/k_E^{\text{off}}}{1 + K_{\text{AE}} (A - A_{\text{min}})} \quad (4)$$

where  $K_{\text{AE}}$  is the strength of AIR-1/ECT-2 inhibition, and  $A_{\text{min}}$  is the minimum level of AIR-1 across all embryo conditions. To fit the parameters in this model, we use the AIR-1 concentration data *with inactivation* (Section 1.1), so that the absolute concentrations are well defined. We set  $\bar{k}^{\text{off}} = 10^{-3} \mu\text{m}^{-2}$ , since this corresponds to a slight weakening of the diffusion without flattening the profile completely. This value of  $\bar{k}^{\text{off}}$  results in the AIR-1 profiles shown in the left panel of Fig. 4. The parameter  $A_{\text{min}} = 1.1$  is set to the minimum AIR-1 concentration across all embryos, and then  $k_E^{\text{on}}/k_E^{\text{off}} = 2.5$  is obtained by fitting the maximum ECT-2 accumulation from experimental data (dhc-1 (RNAi) embryos). The last parameter  $K_{\text{AE}} = 1.3$  is set to match the minimum ECT-2 accumulation of 0.8 when AIR-1 is at its maximum (about 2.8 in dhc-1 (RNAi) embryos). The right panel of Fig. 4 shows the resulting ECT-2 profiles we obtain across different conditions.

Figure 5 compares the resulting output (right panel) to the experimental data (left panel). While we can generally reproduce the trends observed experimentally, the shape of our curve appears to be more of a line, while the experimental data show an S-shaped trend. Indeed, while we correctly predict the ECT-2 accumulation for the “extreme” embryos (dhc-1 (RNAi) and zyg-9 (b224)/tpxl-1(RNAi)), the intermediate embryos have A/P ECT-2 disparities which are smaller than the experimental data. For example, in wild-type embryos, the experiments show an accumulation of 1.8 on the posterior, and 1 on the anterior, while our results show an accumulation of 1.7 on the posterior and 1.4 on the anterior.

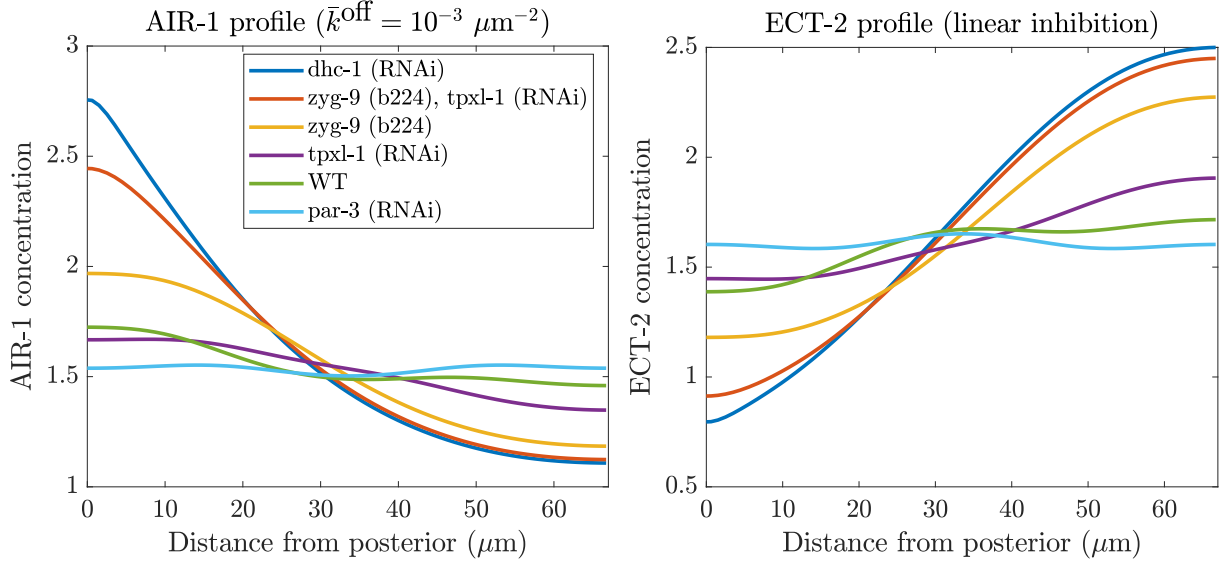


**Figure 4:** AIR-1 and ECT-2 profiles assuming linear inhibition model (4). The AIR-1 profiles are obtained by solving (3) with the different centrosome distances obtained from [7] and  $\bar{k}^{\text{off}} = 10^{-3} \mu\text{m}^{-2}$ . The ECT-2 profiles are then obtained from (4), where we set  $A_{\min} = 1.1$ ,  $k_E^{\text{on}}/k_E^{\text{off}} = 2.5$ , and  $K_{\text{AE}} = 1.3$ .

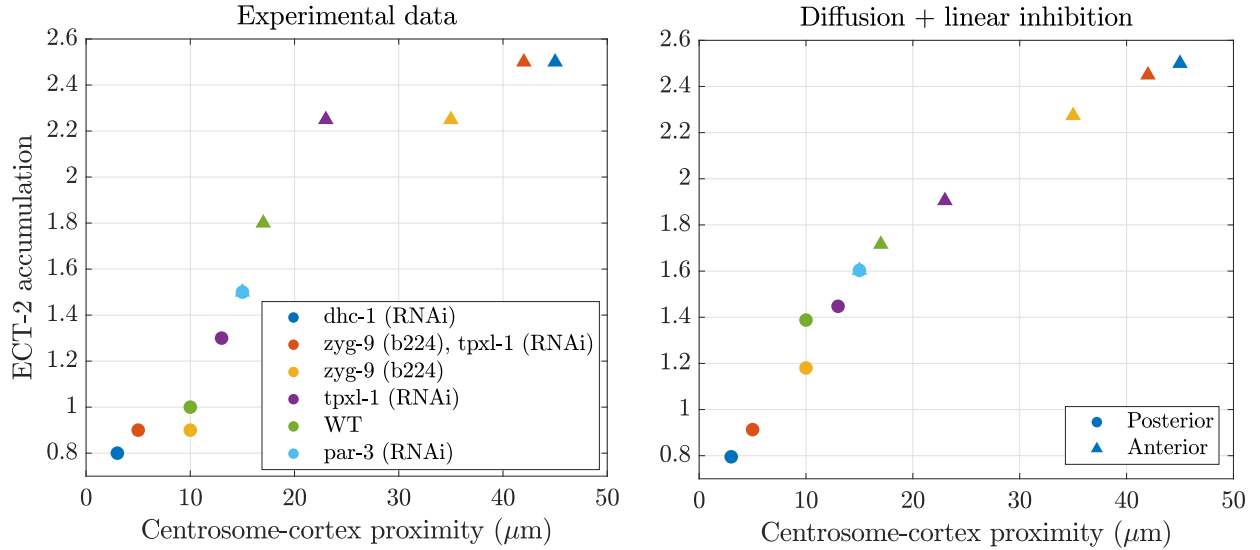


**Figure 5:** Comparing model results to experimental data for embryos with varying treatments (see legend at left). The left plot is a reproduction of [7, Fig. 7A], with some of the redundant embryo treatments deleted for clarity (we reduce multiple replicates to a single symbol by taking a rough average). The right plot shows the results when we consider diffusion of AIR-1 to the cortex, plus linear inhibition of the form (4) (see Fig. 4 for details).

Because we chose parameters to match dhc-1 (RNAi) embryos, their values are correct by design. If, by contrast, we had chosen a larger  $K_{AE}$  to match wild-type embryos, then the model results would be reversed: the wild-type embryos would be correct by design, while the extreme embryos would have A/P ratios which are much *larger* than the experiments. It seems clear that our model is missing a mechanism whereby either:

1. Small changes in ECT-2 concentration induced by diffusion (in an intermediate range) are amplified to become larger.
2. Large changes in ECT-2 concentration induced by diffusion are damped to become smaller.

Since we have not accounted for the resulting actomyosin flows which tend to concentrate ECT-2, we speculate that the first of these options is what is missing from the model. We proceed to study it next.

## 2.1 Flows by myosin

We now explore the possibility that flows due to myosin could propagate smaller ECT-2 asymmetries into larger ones. To do this, we consider the basic model that ECT-2 (through activating  $\rho$ ) activates myosin at the cortex. To minimize the number of parameters, we consider a simplified version of the true dynamics (where ECT-2 signals myosin by activating rho) and formulate a model with two variables,  $E$  (for ECT-2) and  $M$  (for myosin). In a system of units where length is in units of the embryo perimeter  $L$ , time is in units of the bound myosin lifetime  $1/k_M^{\text{off}}$ , and concentrations are scaled to be 1 when all protein is bound, the general equations governing this system can be written as

$$\partial_t E + \sigma_0 \partial_x (vE) = D_E \partial_x^2 E + K_E^{\text{on}} (1 + K_{ME} M) E_c - K_E^{\text{off}} (1 + K_{AE} (A - A_{\min})) E \quad (5a)$$

$$\partial_t M + \sigma_0 \partial_x (vM) = D_M \partial_x^2 M + K_M^{\text{on}} (1 + K_{EM} E) M_c - M - K_{fb} M (t - \tau)^4 \quad (5b)$$

$$v = \ell^2 \partial_x^2 v + \ell \partial_x M \quad (5c)$$

$$E_c = 1 - \int_0^1 E(x) dx \quad M_c = 1 - \int_0^1 M(x) dx. \quad (5d)$$

The first two equations are advection-reaction-diffusion equations which describe the dynamics of ECT-2 and myosin. The term  $\sigma_0 \partial_x (vE)$  describes the rate at which the ECT-2 concentration field is advected by the flow on the cortex, and likewise for the term  $\sigma_0 \partial_x (vM)$  in the myosin equation. In the reaction terms, we assume that myosin recruits ECT-2 from the cytoplasm, and incorporate the

term  $K_{\text{ME}}ME_c$  in the ECT-2 equation. AIR-1 inhibits ECT-2 (by promoting unbinding) according to the relationship (4). For myosin, we assume a basal activation rate plus a rate proportional to the ECT-2 concentration (the term  $K_{\text{EM}}EM_c$ ). We also assume delayed negative feedback of myosin via the term  $K_{\text{fb}}M(t-\tau)^4$ . This is an approximation of a more detailed mechanism whereby actin recruits the RhoGAPs RGA-3/4, which inactivates Rho and myosin [9, 11, 12]. The velocity equation (5c) is a force balance equation where the active ( $\partial_x M$ ) and viscous ( $\partial_x^2 v$ ) forces are balanced by the drag force (proportional to  $v$ ) required to drag myosin at a velocity  $v$  through the cortex [2]. The variable  $\ell$  is the hydrodynamic lengthscale (approximately  $10 \mu\text{m}$  [8]).

### 2.1.1 Parameter estimation

A simple set of assumptions, some of which are based on experimental data, allows us to reduce the dynamics in (5) to two unknown parameters. We do this as follows,

1. The embryo cross section is an ellipse with approximate radii  $27 \mu\text{m}$  and  $15 \mu\text{m}$ , which gives a perimeter  $L = 134.6 \mu\text{m}$  [4] .
2. **The myosin bound lifetime is about 15 s, so  $k_M^{\text{off}} = 1/15 \text{ s}^{-1}$  [5].**
3. We assume that all species have a dimensional diffusion coefficient  $D = 0.1 \mu\text{m}^2/\text{s}$  [4, 5, 10]. Rescaling length by  $L$  and time by  $k_M^{\text{off}}$  gives a dimensionless coefficient  $D_E = D_M = 0.1/(L^2 k_M^{\text{off}}) = 4.6 \times 10^{-5}$ .
4. The ECT-2 lifetime was measured using FRAP to be on the order of a few seconds [7]. We set  $k_E^{\text{off}} = 0.033$ , for a three second lifetime. Rescaling gives  $K_E^{\text{off}} = k_E^{\text{off}}/k_M^{\text{off}} = 0.033/0.12 = 0.275$ .
5. The value of  $K_{\text{EM}}E$  determined what fraction of myosin activation occurs via the ECT-2 pathway. We assume that 2/3 of myosin is activated by ECT-2, so that  $K_{\text{EM}}E = 2$ . Because  $E \approx 0.1$  (see assumption 7), we set  $K_{\text{EM}} = 20$ .
6. We assume that 10% of ECT-2 is bound to the cortex, and 30% of myosin is bound to the cortex [5, Fig. S3j]. This sets  $K_E^{\text{on}} = 0.035$  and  $K_{\text{ME}} = 5$ .
7. For the delayed negative feedback of myosin, we use the parameters determined in [9]. The model there considered rho ( $\rho$ ) and RhoGAP ( $r$ ) as the unknowns, with the production of RhoGAP proportional to  $\rho^3$  and the inhibition of  $\rho$  proportional to  $r\rho$ . Here we coarse-grain this model into a single term, with the inhibition proportional to  $M^4$ . The time delay is



approximately  $\tau = 10$  s (rescaling by  $k_M^{\text{off}}$ , we get  $\tau = 1.2$  in units of myosin lifetime), as obtained from experimental data [9]. The feedback strength is obtained by assuming an equilibrium of  $r$  in the equations of [9] (neglecting the basal binding rate), which gives (in their notation)  $K_{\text{fb}} = k_{\text{GAP}} (k_r^{\text{ass}}/k_r^{\text{diss}}) = 0.1(0.245/0.047) = 0.52/\text{s}$ . Rescaling by  $k_M^{\text{off}}$  gives  $K_{\text{fb}} = 4.3$  in our model.

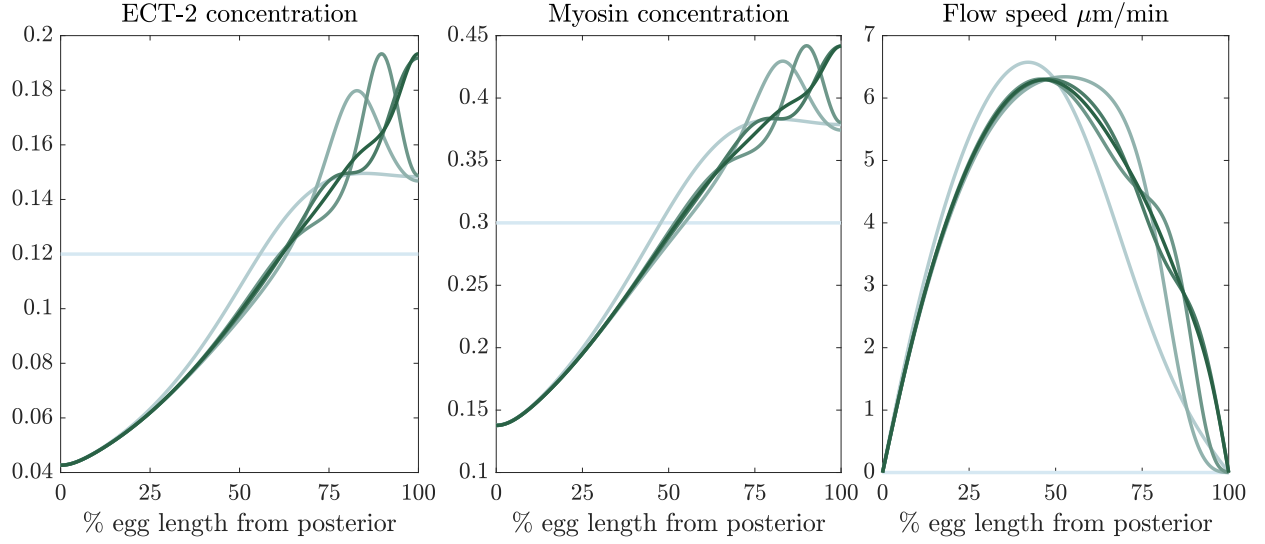
This systematic fitting procedure reduces the dynamics to two parameters:  $K_{\text{AE}}$ , which describes the rate at which AIR-1 inhibits ECT-2, and  $\sigma_0$ , which is the speed of flows induced by myosin gradients. By manipulating these two parameters, we can model situations where ECT-2 gradients are due to AIR-1 alone (this is Fig. 5, where  $K_{\text{AE}} = 1.3$  and  $\sigma_0 = 0$ ), or where there is substantial amplification by flows. In the extreme case when  $K_{\text{AE}} = 0$  and  $\sigma_0$  is sufficiently large, we will get oscillatory dynamics, with peaks of myosin occurring at random places, in accordance with the model of [9]. We need a sufficiently large  $K_{\text{AE}}$  to ensure that the myosin peaks are in the right places.

Our approach is to start with a uniform concentration of ECT-2 and myosin, then apply the AIR-1 signal and watch the dynamics for ten minutes (long enough to reach a rough steady state, as shown in Fig. 6). To find a combination of  $K_{\text{AE}}$  and  $\sigma_0$  that best satisfies the data, we start by fixing  $K_{\text{AE}}$ , then adjust  $\sigma_0$  so that *dhc-1* embryos have the experimental A/P ratio ( $\approx 3.2$ ) of ECT-2 at the end of the simulation. We accept a pair of parameters  $(K_{\text{AE}}, \sigma_0)$  if these same parameters give an A/P ratio around 1.8 in wild-type embryos as well. Figure 6 shows the dynamics over ten minutes with our chosen parameters  $K_{\text{AE}} = 0.6$  and  $\sigma_0 = 0.2$ . In *dhc-1* embryos, there is a single peak in the ECT-2 and myosin concentration which forms at around 75% embryo length (from the posterior), while in wild-type there are two peaks of ECT-2: one at the midline, and one at the anterior pole.

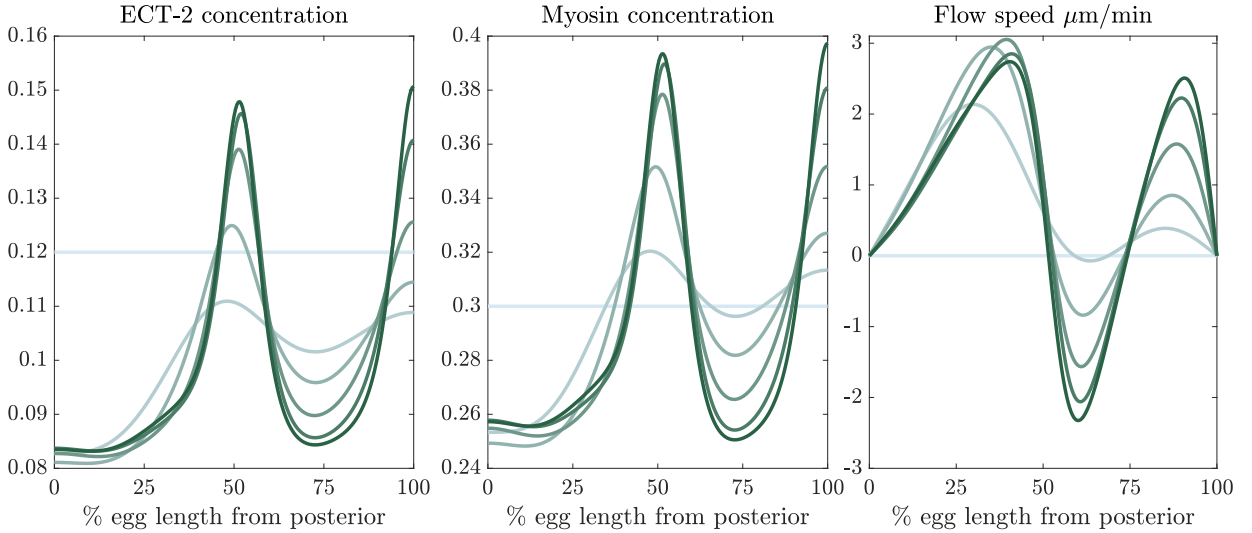
To compare our results with flow to the experimental data, we define an accumulation on the anterior cortex as the maximum ECT-2 concentration on the anterior 25% of the embryo length, and likewise for the posterior. Figure 7 shows how our asymmetry results compare to the experimental data. Compared to the previous data in Fig. 5, our data show more of an “S” shape, qualitatively (and quantitatively, for the most part) reproducing the shape obtained in experiments.

## 2.2 Attempting a larger lengthscale (viscosity)

When we model polarization, it might be helpful to stretch the hydrodynamic lengthscale  $\ell$  so that disturbances propagate farther along the A/P axis. We first try to implement this for cytokinesis



(a) *dhc-1* (RNAi)



(b) Wild type

**Figure 6:** Trajectory with flows over 10 minutes of simulation time (cytokinesis conditions). We show the ECT-2 concentration, myosin concentration, and flow speed at times  $t = 0$  (lightest lines),  $t = 2, 4, 6, 8$ , and  $t = 10$  (darkest lines). (a) *dhc-1* embryos, where the AIR-1 signal is stronger and concentrated almost entirely in the posterior (see Fig. 4). (b) Wild-type embryos, where the AIR-1 has a local minimum at the midline of the cell, plus an absolute minimum at the anterior pole.

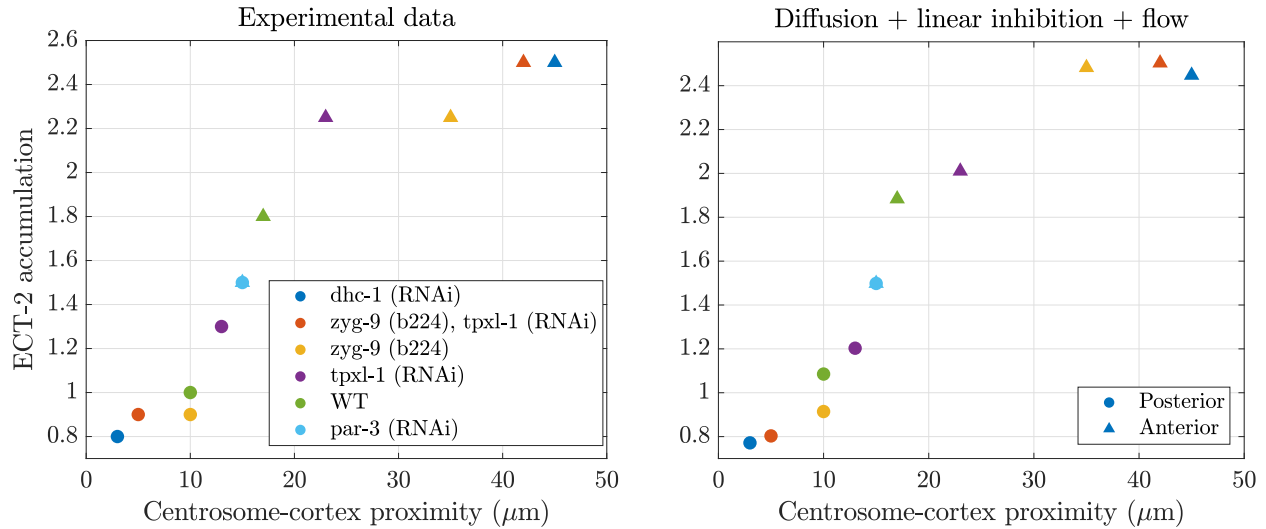
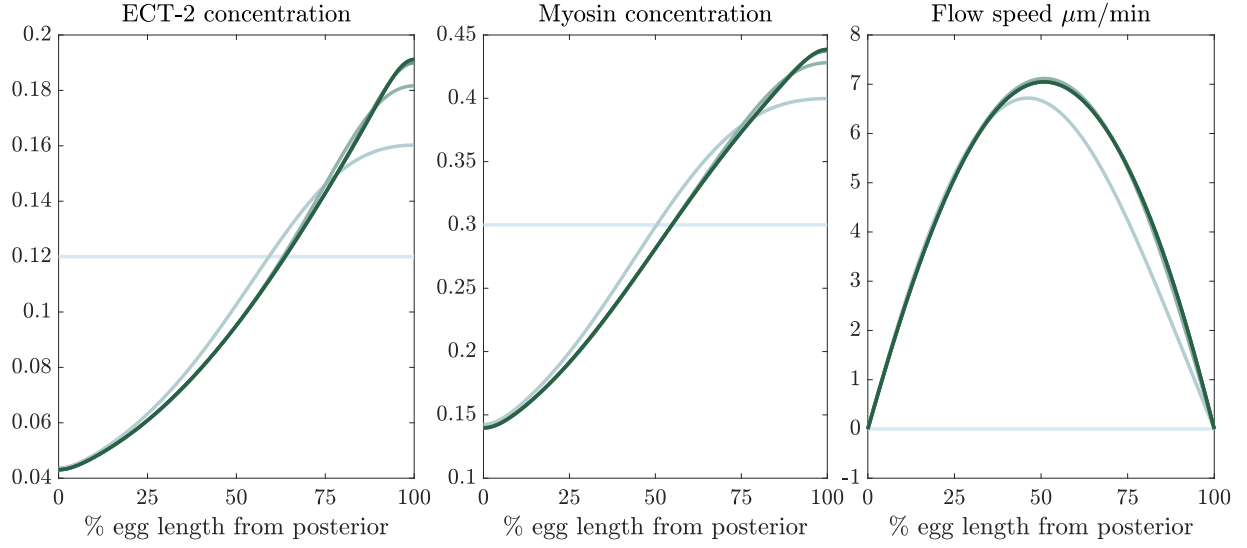


**Figure 7:** Comparing model results with myosin flows to experimental data for embryos with varying treatments (see legend at left). The left plot is a reproduction of [7, Fig. 7A], with some of the redundant embryo treatments deleted for clarity (we reduce multiple replicates to a single symbol by taking a rough average). The right plot shows the results when we consider diffusion of AIR-1 to the cortex, then run the model (5) to steady state with our chosen parameters. Unlike the model without flow (Fig. 5), the model with flow reproduces the “S” shape observed in experiments.

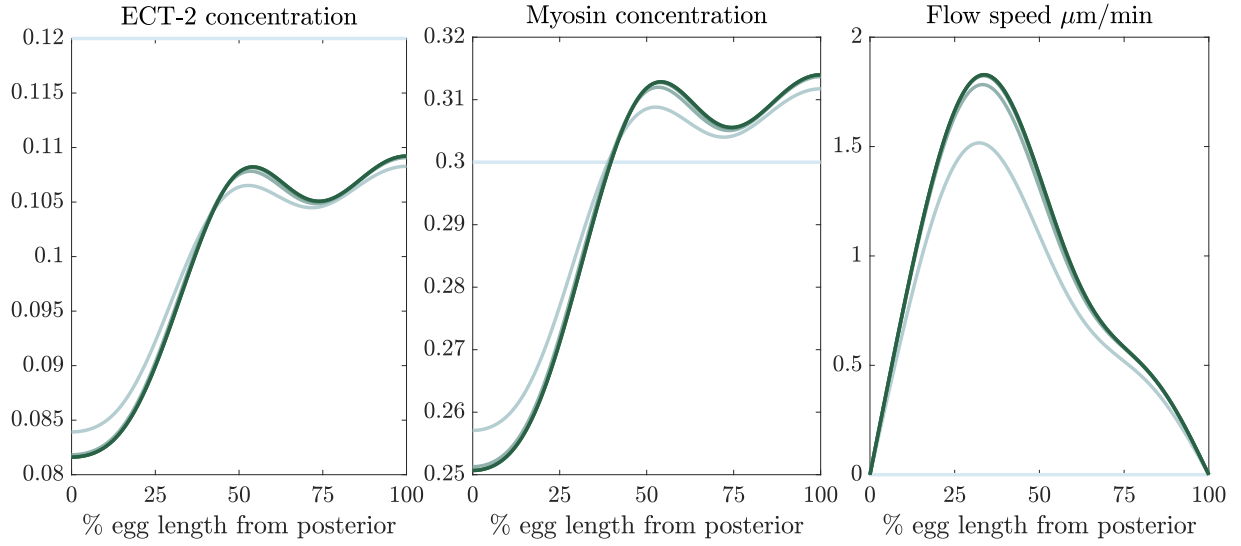
by keeping all parameters fixed and setting  $\ell = 0.2$  (or 20% embryo length). The results of this are shown in Fig. 8. For the *dhc-1* embryos, there is little change from Fig. 6(a); the flow is always anterior-directed and has the same magnitude. This occurs because the profiles are sufficiently smooth, and so they don’t have strong viscous stresses.

By contrast, the wild type profile in Fig. 8 (longer lengthscale) looks completely different from the one with the default parameters (Fig. 6(b)). Because the original velocity profile has multiple peaks, it exhibits high rates of strain near the equator. These rates of strain get smoothed out when we increase the lengthscale. Now the flow profile is entirely anterior-directed, and there is no longer peak myosin at the equator. Because of the weaker flow and myosin activity, the ECT-2 ratio drops from 1.7 for  $\ell = 0.1$  to 1.2 when  $\ell = 0.2$ .

Interestingly, because changing the lengthscale affects wild-type embryos but not *dhc-1* embryos, it becomes impossible to find a pair  $(K_{\text{AE}}, \sigma_0)$  for which the A/P ratio of ECT-2 is correct for both *dhc-1* and wild type embryos. Figure 8 shows the case when the *dhc-1* ratio is correct and the ECT-2 ratio is too low; sets of parameters for which the ECT-2 ratio is correct gives very large (roughly 10) ratios for *dhc-1*.



(a) *dhc-1* (RNAi)



(b) Wild type

**Figure 8:** Trajectory with flows over 10 minutes of simulation time (cytokinesis conditions) *doubling the hydrodynamic lengthscale (quadrupling the viscosity)*. This is a repeat of Fig. 6 with  $\ell = 0.2$  (or 20% embryo length) instead of  $\ell = 0.1$ . Comparing the figures, the *dhc-1* embryos are not strongly affected, while there is a huge effect on wild type embryos.

### 3 Polarization

Here we attempt to apply our model, with the same parameters, to the process of cell polarization. We begin with the diffusion calculation to establish the profile of AIR-1, then see how this propagates in our myosin/ECT-2 model.

#### 3.1 Diffusion of AIR-1

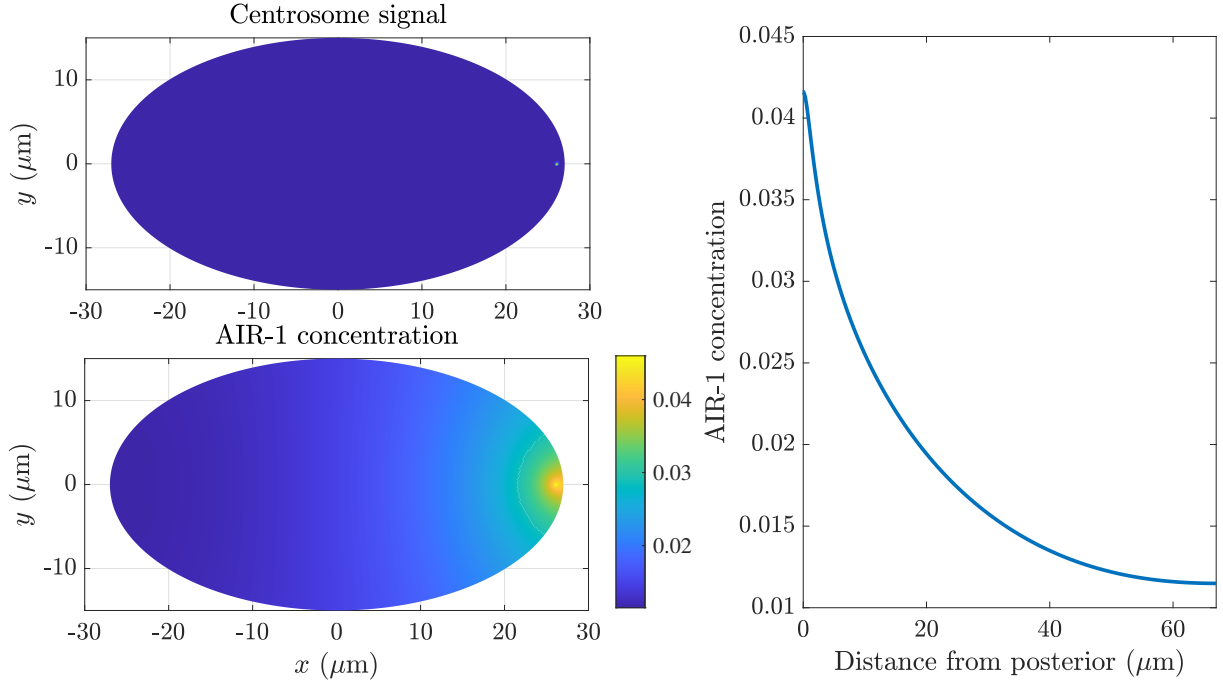
In cell polarization, *both* centrosomes sit very close to the posterior cortex (about  $1\text{ }\mu\text{m}$  away [3]). The centrosomes have a smaller size (about  $0.2\text{ }\mu\text{m}$ , so we set  $\sigma_c = 0.1\text{ }\mu\text{m}$ ). They also contain substantially less total AIR-1; here we assume that the amount scales with the area, so that  $C_0 = 0.01$  for polarization. Figure 9 shows the resulting AIR-1 concentration profile (the solution of (3) with  $\bar{k}^{\text{off}} = 10^{-3}\text{ }\mu\text{m}^{-2}$  once again) across the embryo and along the boundary. We observe a change in AIR-1 of only 0.03 from one side of the embryo to the other, which is substantially *smaller* than what we observed in cytokinesis. Considering that ECT-2 becomes asymmetrically enriched during polarization at the same levels as in cytokinesis, this underscores the need to have a mechanism to amplify the asymmetries.

#### 3.2 The myosin response

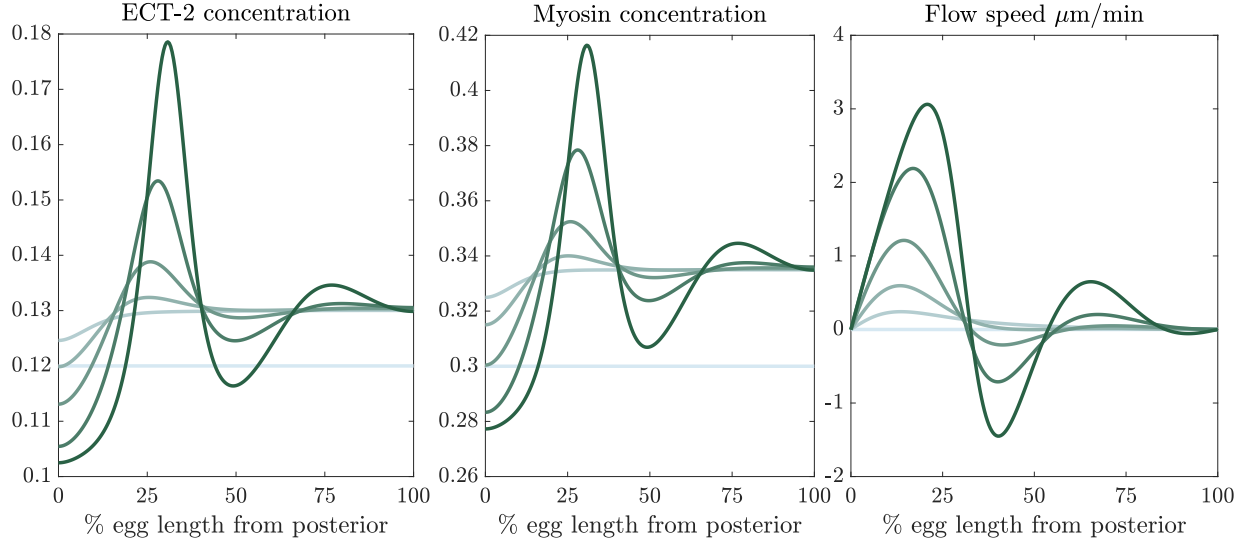
We now simulate the response to the AIR-1 signal using the equations (5). We use all of the same parameters as for cytokinesis, with the exception of  $A_{\min}$ , which is the “base” concentration of AIR-1, at which there is no effect on ECT-2. We previously set this value to be the smallest value of the AIR-1 concentration across all embryos in cytokinesis; here we use the minimum concentration for polarization, which, according to Fig. 9 is  $A_{\min} = 0.01$ .

Figure 10 shows the response of the system to the AIR-1 signal, which in polarization is highly localized to the posterior cortex (see Fig. 9). In the first ten minutes of simulation time (which is longer than polarity establishment phase), a peak in myosin and ECT-2 forms immediately next to the posterior pole. At  $t = 10$  minutes, this peak has an A/P asymmetry of roughly 2. Later times show formation of additional peaks, and a steady state emerges with a set of three peaks of the same size. The overall ECT-2 asymmetry is roughly 2.5, which is slightly larger than what is measured experimentally (at most 1.8).

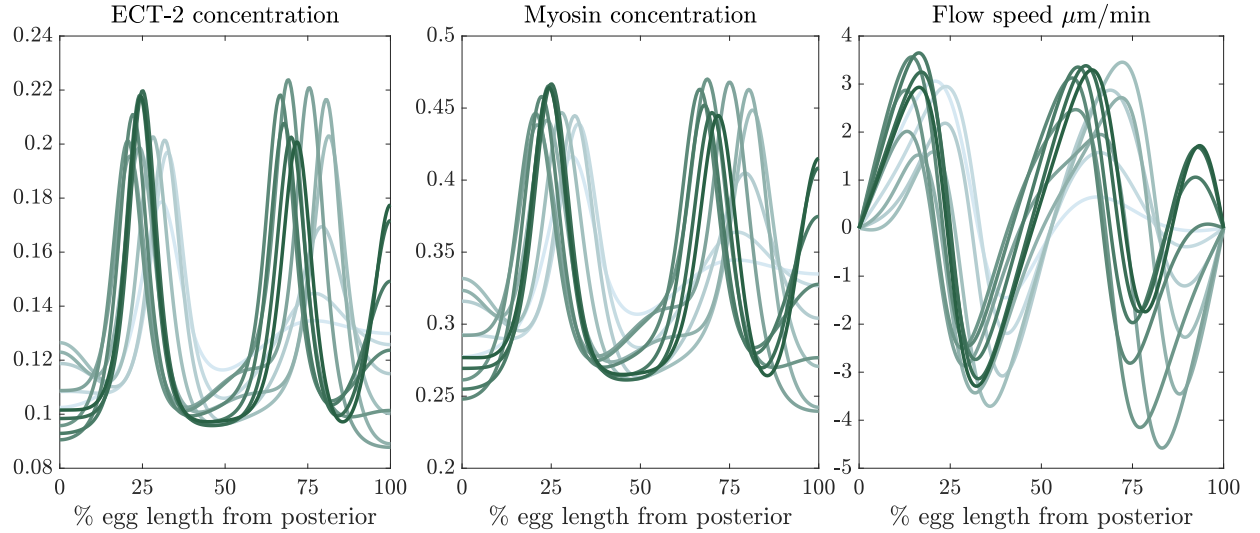
The major qualitative issue with this model is the location of the peaks, and the inability to move the peak that initially forms near the posterior pole. In experiments, we might expect the



**Figure 9:** AIR-1 signal during polarization. In polarization, both centrosomes sit on the posterior cortex (we assume  $1\ \mu\text{m}$  away), have smaller size (about  $0.2\ \mu\text{m}$ , so we set  $\sigma_c = 0.1\ \mu\text{m}$ ), and contain less ( $C_0 = 0.01$ ) AIR-1 than in cytokinesis (see plot at top left). The resulting concentration profile is shown across the entire embryo (bottom left) and along the embryo boundary (right).



(a) First 10 minutes (establishment phase)



(b) Next 20 minutes (to steady state)

**Figure 10:** Dynamics for cell polarization model. We run the model (5), which we previously fit to cytokinesis, with the same parameters, changing only the AIR-1 profile to the polarization cue obtained in Section 3.1. We show the dynamics at two minute intervals, starting from  $t = 0$ , over (a) the first ten minutes (which is at most the length of polarity establishment phase) and (b) the next twenty minutes (which establishes a steady state but is of little relevance in practice). Darker lines show later times.

dynamic reorganization of PAR proteins to shift the location of the peak in ECT-2. Because this model does not account for PAR proteins, peaks that initially form at a fixed location will not move, because the signals upstream of them do not change. The result is the profiles shown in Fig. 10.

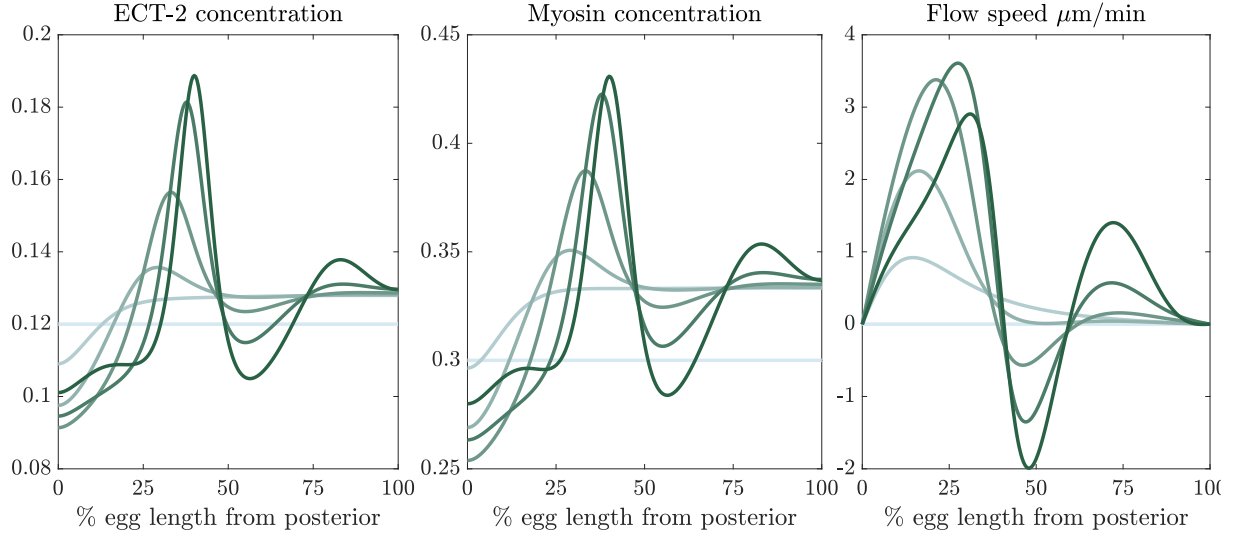
### 3.2.1 Trying a larger AIR-1 signal

To demonstrate that the issue with polarization is the propagation of the AIR-1 signal and not the signal itself, we consider a repeat of the entire process with the centrosomes having four times as much AIR-1. The resulting dynamics are shown in Fig. 11. In the first ten minutes of polarization, the peak in ECT-2 moves further towards the midline of the cell than in Fig. 10(a), but the effect is slight; at most 10% embryo length. At later times, multiple peaks in ECT-2 and myosin return. These tend to travel about the anterior more than previously observed with a lower ECT-2 signal, but the qualitative effect is the same: the ECT-2 disturbance near the posterior simply does not propagate into the anterior. Rather, the disturbance only gets propagated about one hydrodynamic lengthscale ( $13\text{ }\mu\text{m}$  is about 25% of the embryo length).

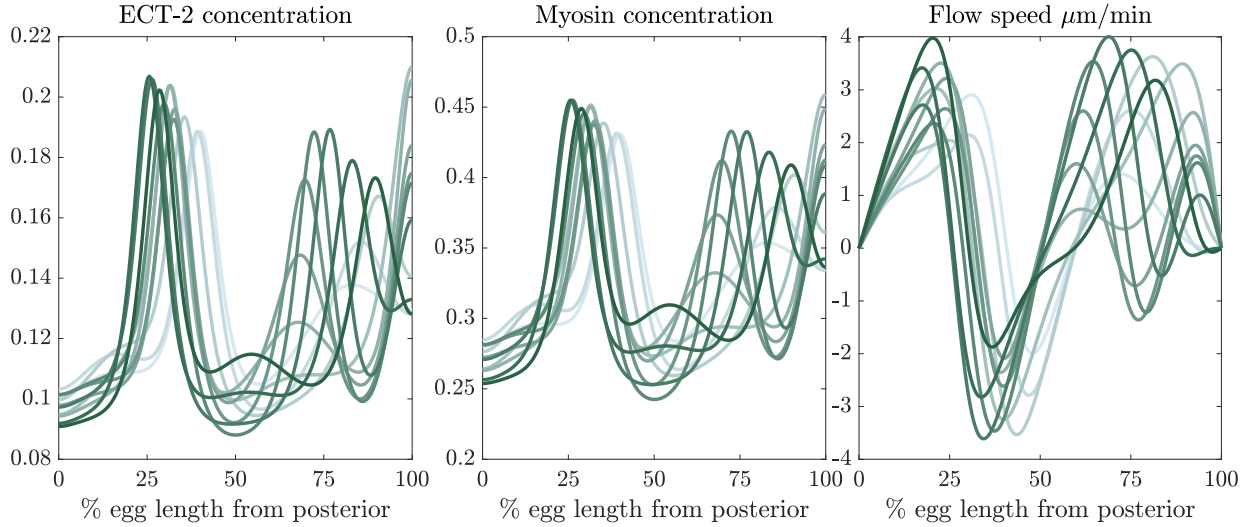
## References

- [1] Katayoun Afshar, Michael E Werner, Yu Chung Tse, Michael Glotzer, and Pierre Gönczy. Regulation of cortical contractility and spindle positioning by the protein phosphatase 6 pph-6 in one-cell stage *c. elegans* embryos. *Development*, 137(2):237–247, 2010.
- [2] Justin S Bois, Frank Jülicher, and Stephan W Grill. Pattern formation in active fluids. *Biophysical Journal*, 100(3):445a, 2011.
- [3] Carrie R Cowan and Anthony A Hyman. Centrosomes direct cell polarity independently of microtubule assembly in *c. elegans* embryos. *Nature*, 431(7004):92–96, 2004.
- [4] Nathan W Goehring, Philipp Khuc Trong, Justin S Bois, Debanjan Chowdhury, Ernesto M Nicola, Anthony A Hyman, and Stephan W Grill. Polarization of par proteins by advective triggering of a pattern-forming system. *Science*, 334(6059):1137–1141, 2011.
- [5] Peter Gross, K Vijay Kumar, Nathan W Goehring, Justin S Bois, Carsten Hoege, Frank Jülicher, and Stephan W Grill. Guiding self-organized pattern formation in cell polarity establishment. *Nature physics*, 15(3):293–300, 2019.





(a) First 10 minutes (establishment phase)



(b) Next 20 minutes (to steady state)

**Figure 11:** Dynamics for cell polarization model when the AIR-1 signal is four times stronger. There is a slight shift in the ECT-2 peak initially, but the final steady state is more or less the same (it is a little more chaotic). This reflects the fact that the AIR-1 signal, which is very small in polarization, simply triggers the system into its peaked state.

- [6] Sachin Kotak, Katayon Afshar, Coralie Busso, and Pierre Gönczy. Aurora a kinase regulates proper spindle positioning in *c. elegans* and in human cells. *Journal of cell science*, 129(15):3015–3025, 2016.
- [7] Katrina M Longhini and Michael Glotzer. Aurora a and cortical flows promote polarization and cytokinesis by inducing asymmetric ect-2 accumulation. *Elife*, 11:e83992, 2022.
- [8] Mirjam Mayer, Martin Depken, Justin S Bois, Frank Jülicher, and Stephan W Grill. Anisotropies in cortical tension reveal the physical basis of polarizing cortical flows. *Nature*, 467(7315):617–621, 2010.
- [9] Jonathan B Michaux, François B Robin, William M McFadden, and Edwin M Munro. Excitable rhoa dynamics drive pulsed contractions in the early *c. elegans* embryo. *Journal of Cell Biology*, 217(12):4230–4252, 2018.
- [10] François B Robin, William M McFadden, Baixue Yao, and Edwin M Munro. Single-molecule analysis of cell surface dynamics in *caenorhabditis elegans* embryos. *Nature methods*, 11(6):677–682, 2014.
- [11] Cornelia Schmutz, Julia Stevens, and Anne Spang. Functions of the novel rhogap proteins rga-3 and rga-4 in the germ line and in the early embryo of *c. elegans*. 2007.
- [12] Stephanie Schonegg, Alexandru T Constantinescu, Carsten Hoege, and Anthony A Hyman. The rho gtpase-activating proteins rga-3 and rga-4 are required to set the initial size of par domains in *caenorhabditis elegans* one-cell embryos. *Proceedings of the National Academy of Sciences*, 104(38):14976–14981, 2007.